Catalysis Today 164 (2011) 358–363

Contents lists available at ScienceDirect

Catalysis Today

journal homepage: www.elsevier.com/locate/cattod

Synthesis and catalytic properties of porous Nb–Mo oxide solid acid

Caio Tagusagawa[a], Atsushi Takagaki[a], Ai Iguchi[b], Kazuhiro Takanabe[a], Junko N. Kondo[b], Kohki Ebitani[c], Takashi Tatsumi[b], Kazunari Domen[a,*]

[a] Department of Chemical System Engineering, School of Engineering, The University of Tokyo, 7-3-1, Hongo, Bunkyo-ku, Tokyo 113-7656, Japan
[b] Chemical Resources Laboratory, Tokyo Institute of Technology, 4259 Nagatsuta Midori-ku, Yokohama 226-8503, Japan
[c] School of Materials Science, Japan Advanced Institute of Science and Technology (JAIST), 1-1 Asahidai, Nomi, Ishikawa 923-1292, Japan

ARTICLE INFO

Article history:
Available online 11 November 2010

Keywords:
Solid acid
Porous metal oxide
Friedel–Crafts alkylation
FT-IR

ABSTRACT

Several porous Nb_xMo_{10-x} mixed oxides prepared from $NbCl_5$ and $MoCl_5$ in the presence of block copolymer surfactant Pluronic P-123 were examined as potential solid acid catalysts. Amorphous mesoporous structures were observed in samples with x from 10 to 9, whereas samples with higher Mo concentrations (x = 3–8) formed large pores by inter-particle voids and a non-porous structures with crystallized molybdenum oxide (MoO_3) were observed in samples with x from 0 to 2. The acid strength increased with increasing the Mo content in Nb_xMo_{10-x} oxides, which was determined by NH_3 temperature-programmed desorption (NH_3-TPD) and Fourier transform infrared (FT-IR) spectroscopy using pyridine as a probe molecule. Porous Nb_3Mo_7 oxide exhibited the highest acid-catalytic activity for the Friedel–Crafts alkylation of anisole due not only to mole ratio of Nb/Mo but also to pore structure.

1. Introduction

The acidities of bulk metal oxides and mixed oxides have been widely studied as a promising substitute for liquid acid. Hydrated niobium oxide, also called niobic acid is a well known bulk metal oxide with strong Brønsted acidity and water tolerant solid acid. Therefore deep study on niobium oxide and tantalum oxide has been investigated on their acid sites characterizations and catalytic activities [1–8]. However, its application to acid-catalyzed reactions has not yet been performed sufficiently.

Mixed metal oxides are known to exhibit higher reaction activity and stronger acidity than single metal oxides. To explain the acid generation of binary oxides [9,10], Tanabe et al. proposed the hypothesis, where acid site generation is caused by an excess of a negative or positive charge in the model structure of a binary oxide for chemically mixed oxides. Actually, the hypothesis agrees with 90% of the 31 kinds of binary oxides composed principally by TiO_2, ZnO, Al_2O_3, SiO_2 and ZrO_2 [11]. Nb_2O_5–MoO_3 and Nb_2O_5–WO_3 reported by Niwa and co-workers exhibit very strong acid strength and catalytic activity for Friedel–Crafts alkylation of anisole with benzyl alcohol [12]. Their activities are much higher than that of other niobium containing metal oxides (Nb_2O_5/SiO_2, Nb_2O_5/TiO_2, Nb_2O_5/MgO and Nb_2O_5). They suggested two hypotheses for the formation of active species; an isomorphous replacement model [13], which is known in the zeolites, or formation of heteropoly compounds like the H_3PO_4–WO_3–Nb_2O_5 [14,15].

To improve the rates of metal oxide acid catalysis, mesoporous structured solid acids have been widely studied [16–21]. High surface area mesopores in oxide enable the reactants to access acid sites, exhibiting high activity and selectivity, principally for sulfated mesoporous niobium [20] and tantalum oxides [21,22]. Our previous studies on mesoporous Nb–W and Ta–W oxide solid acids [23,24] have revealed that wormhole-type mesoporous Nb–W and Ta–W oxides can be applied as recyclable and highly active solid acid catalysts for Friedel–Crafts alkylation, hydrolysis of disaccharides, and esterification. The reaction rate and the acid strength increased gradually with the addition of W, reaching the highest reaction rate with mesoporous Nb_3W_7 and Ta_3W_7 oxides, which exceeded the reaction rate of ion-exchange resins, zeolites, and non-mesoporous metal oxides.

In the present study, porous Nb–Mo mixed oxides with different Nb and Mo concentrations were examined as novel solid acid catalysts. Previous study demonstrated that isomorphous replacement of Nb^{5+} and Ta^{5+} by higher-valence W^{6+} cations formed strong Brønsted acid sites in W-enriched samples, resulting in a highly active mesoporous solid acid [23,24]. Therefore, porous Nb–Mo mixed oxide was tested in an attempt to obtain a more effective solid acid than non-porous Nb_2O_5–MoO_3 oxide. The acid properties of porous Nb–Mo oxides were evaluated by NH_3 temperature-programmed desorption (NH_3-TPD) and Fourier transform infrared (FT-IR) spectroscopy. The acid catalytic activity of porous Nb–Mo oxides with different Nb–Mo concentrations were examined dur-

* Correspondence author: Tel.: +81 3 5841 1148; fax: +81 3 5841 8838.
E-mail address: domen@chemsys.t.u-tokyo.ac.jp (K. Domen).

0920-5861/$ – see front matter © 2010 Elsevier B.V. All rights reserved.
doi:10.1016/j.cattod.2010.10.049

ing liquid-phase Friedel–Crafts alkylation of anisole and the results are compared with those of conventional solid acids.

2. Experimental

2.1. Preparation of porous metal oxides

Porous $Nb_xMo_{(10-x)}$ oxides were prepared from niobium pentachloride $NbCl_5$ (99.99%, Kojundo Chemical Laboratory Co., Ltd.) and molybdenum pentachloride $MoCl_5$ (99.99%, Kojundo Chemical Laboratory Co., Ltd.). Poly block copolymer surfactant Pluronic P-123 ($(HO(CH_2CH_2O)_{20}–(CH_2CH(CH_3)O)_{70}–(CH_2CH_2O)_{20}H$, Aldrich) was used as a structure-directing agent (SDA). Porous $Nb_xMo_{(10-x)}$ oxide was synthesized by dissolving 1 g of P-123 in 10 g of dehydrated 1-propanol, and adding $NbCl_5$ and $MoCl_5$ (total of 6 mmol metal chloride) for porous $Nb_xMo_{(10-x)}$ and 7 mmol $NbCl_5$ for mesoporous Nb oxide with vigorous stirring. Water (30 mmol) was added to the solution with further stirring. The resulting sol was gelled in a Petri dish at 313 K for 10–14 days. The aged gel samples were then treated at 673 K for 10 h in static air to remove the SDA.

2.2. Characterization

Samples were characterized by N_2 desorption (BEL Japan, BELSORP-miniII), X-ray diffraction (XRD; RINT-UltimaIII, Rigaku), and scanning electron microscopy (SEM; S-4700, Hitachi). The Brunauer–Emmett–Teller (BET) surface area was estimated over a relative pressure (P/P_0) range of 0.05–0.30. The pore size distribution was obtained from analysis of the adsorption branches of the isotherms using the Barrett–Joyner–Halenda (BJH) method and the small-angle powder X-ray diffraction pattern.

The acid properties of the samples were determined by NH_3-TPD (acid strength and concentration of sites) using a TPD-1-AT instrument (BEL Japan) equipped with a quadrupole mass spectrometer and FT-IR (acid type: Brønsted and Lewis acid) spectroscopy (FT-IR; Jasco, FT/IR-6200). For TPD measurement, a 20 mg sample was heated at 423 K for 1 h under helium flow, exposed to NH_3 at 373 K for adsorption, and finally heated at 2 K min^{-1}. For IR spectroscopic measurements, the samples were evacuated in a conventional gas-circulation system at 423 K for 1 h, and then pyridine was introduced into the system to be adsorbed on the acid sites for the study of the acid properties.

2.3. Acid-catalyzed reactions

Friedel–Crafts alkylation was performed using 0.2 g of catalyst, 100 mmol of anisole, and 10 mmol of benzyl alcohol in an oil bath at 373 K for 1 h. The products (ortho-benzylanisole, para-benzylanisole, and dibenzylether) were analyzed by flame ionization gas chromatography (GC-2014, Shimadzu), using a capillary column (J&W Scientific-DB-FFAP, length 30 m, i.d. 0.25 mm, and film 0.25 μm).

The activities of niobic acid ($Nb_2O_5•nH_2O$), Nb_2O_5–MoO_3, ion-exchange resins (Amberlyst-15 and Nafion NR50), and H-Beta zeolite (SiO_2/Al_2O_3 = 25, JRC-Z-HB25 supplied from the Catalysis Society of Japan (Japan Reference Catalyst)) were used for comparison. Non-porous Nb_2O_5–MoO_3 was prepared as follows. $Nb_2O_5•nH_2O$ (n = 3.8, measured by TG) kindly supplied by CBMM Co. and $(NH_4)_6Mo_7O_{24}•4H_2O$ were dissolved in oxalic acid solution and distilled water, respectively, at 353 K. The solutions were then mixed and stirred vigorously at 353 K. After drying, the obtained materials were calcined at 673 K for 3 h to yield Nb–Mo mixed oxides.

3. Results and discussion

3.1. Structure of porous $Nb_xMo_{(10-x)}$ metal oxides

The presence of a porous structure was evaluated from N_2 sorption isotherms (Fig. 1), XRD patterns (Fig. 2) and SEM images (Fig. 3). N_2 sorption isotherms (Fig. 1) indicated the presence of porous structures in samples with x = 3–10. These exhibited a typical type-IV pattern with an H1-type hysteresis loop at high relative pressures for mesopores with high Nb (x = 9–10) concentrations. Hysteresis loops similar to the H2-type were observed for sam-

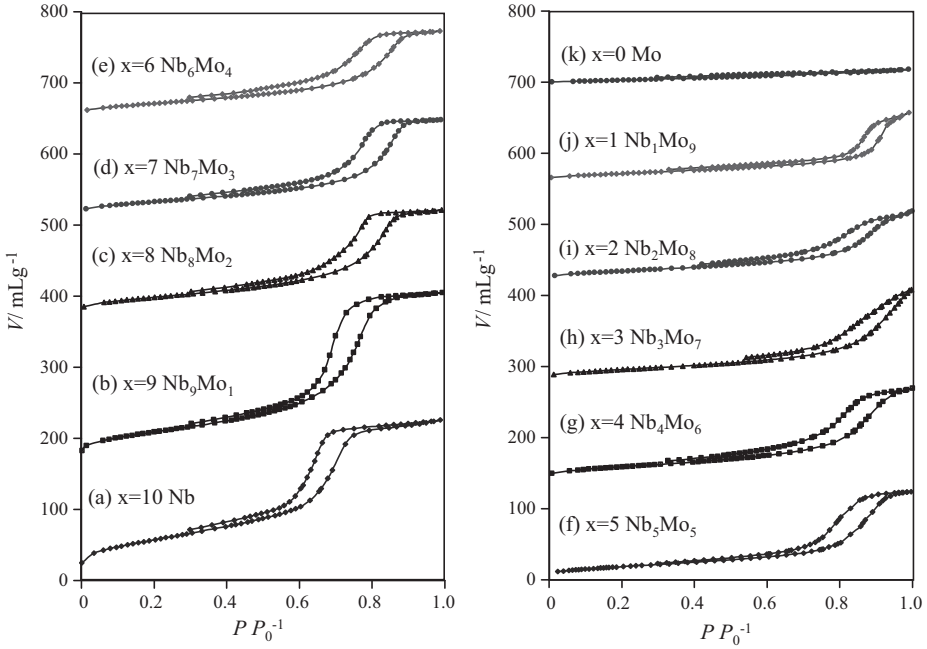

Fig. 1. N_2 sorption isotherms of mesoporous (a) Nb, (b) Nb_9Mo_1, porous (c) Nb_8Mo_2, (d) Nb_7Mo_3, (e) Nb_6Mo_4, (f) Nb_5Mo_5, (g) Nb_4Mo_6, (h) Nb_3Mo_7 and non-porous (i) Nb_2Mo_8, (j) Nb_1Mo_9 and (k) Mo oxides.

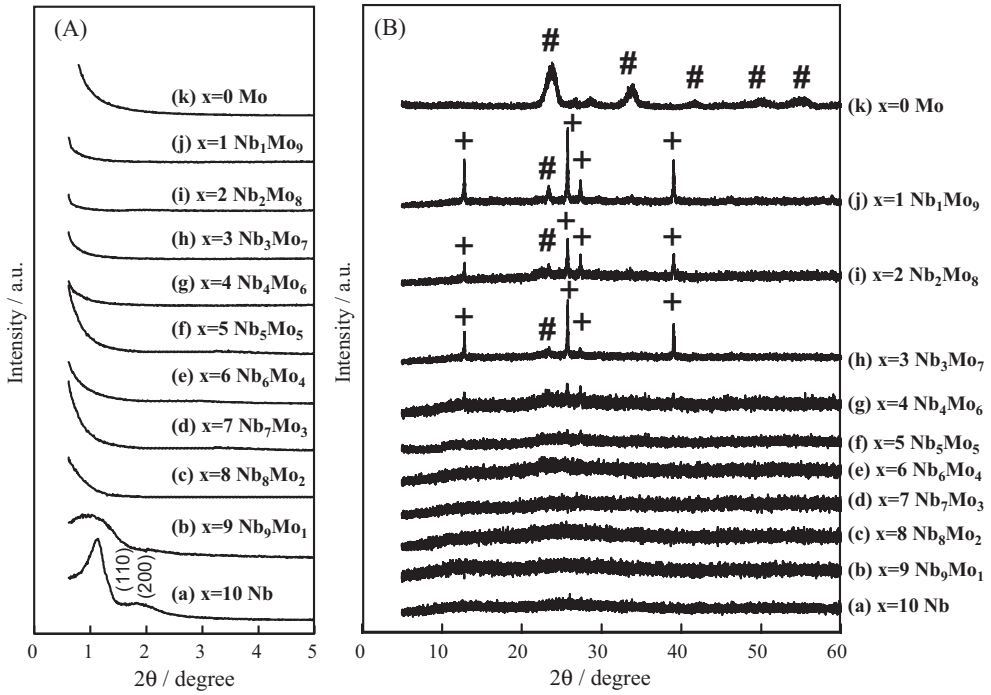

Fig. 2. (A) Low and (B) wide-angle powder XRD patterns for mesoporous (a) Nb, (b) Nb_9Mo_1 and non-mesoporous (c) Nb_8Mo_2, (d) Nb_7Mo_3, (e) Nb_6Mo_4, (f) Nb_5Mo_5, (g) Nb_4Mo_6, (h) Nb_3Mo_7, (i) Nb_2Mo_8 oxides, (j) Nb_1Mo_9 and (k) Mo oxides (+, $Mo_3Nb_2O_{14}$; #, MoO_3).

ples with x values from 3 to 8. The small-angle XRD patterns (Fig. 2) contained peaks attributable to mesopores for $Nb_xMo_{(10-x)}$ oxides with x values from 9 to 10. Peaks attributed to (1 1 0) and (2 0 0) of the two-dimensional hexagonal structure were observed from an $x = 10$ sample (mesoporous Nb_2O_5), which was consistent with previous studies [23]. The small-angle XRD peaks indicating mesoporous structure could not be observed for samples with x values form 0 to 8. Wide-angle powder XRD patterns revealed the presence of an amorphous structure in samples with $x = 4$–10, $Mo_3Nb_2O_{14}$ in samples with $x = 4$–1 and crystallized molybdenum oxide (MoO_3) in Mo-rich samples with $x = 3$–0. SEM images of the prepared porous oxides are shown in Fig. 3. The mesoporous Nb oxide had hexagonally structured mesopores, as observed in the XRD pattern. Nb_7Mo_3, Nb_5Mo_5, and Nb_3Mo_7 oxides had large pores formed by inter-particle voids, different from mesopores observed at mesoporous Nb oxide, supporting both N_2 sorption isotherms (formation of pores) and XRD patterns results (no mesopores). A crystallized MoO_3 was observed in the Mo oxides, supporting the XRD results.

Characterization of the pores was conducted by both Brunauer–Emmett–Teller (BET) (surface area estimation) and Barrett–Joyner–Halenda (BJH) (pore size distributions) methods. Fig. 4 shows the variation in surface area and pore volume versus Mo concentration. The BET surface area decreased gradually from 200 (mesoporous Nb oxide) to 21 $m^2\,g^{-1}$ (non-porous Mo oxide) with increasing Mo content, up to $x = 0$, due to the formation of

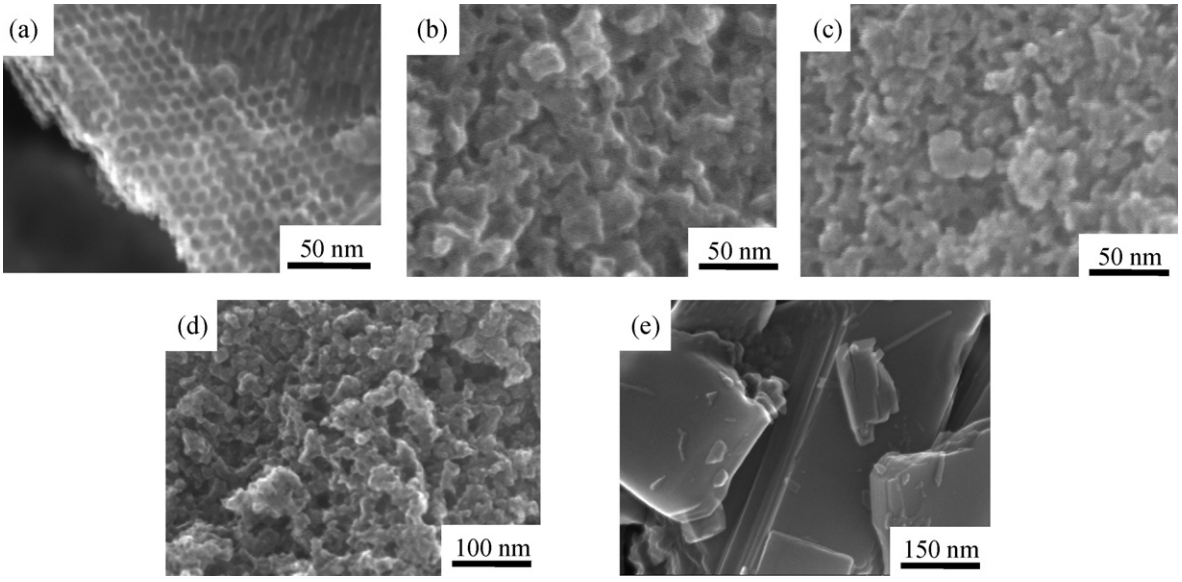

Fig. 3. SEM images of mesoporous (a) Nb, porous (b) Nb_7Mo_3, (c) Nb_5Mo_5, (d) Nb_3Mo_7 oxides and non-porous e) Mo oxides.

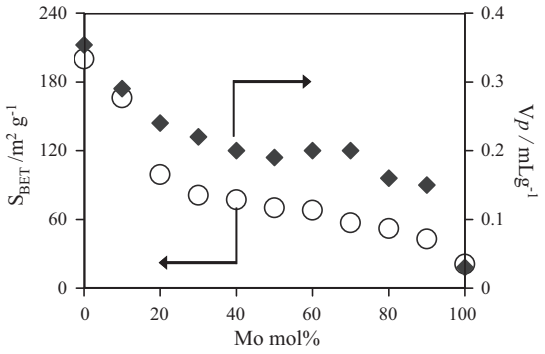

Fig. 4. BET surface areas (m^2/g) and pore volumes (μL/g) of porous Nb_xMo_{1-x} oxides.

crystallized $Mo_3Nb_2O_{14}$ and MoO_3 oxides in the Mo-rich samples. Aggregation and crystallization resulted in the destruction of the original mesoporous structure and the development of larger pores (between 10.6 and 18.6 nm) for $Nb_xMo_{(10-x)}$ oxides (x = 1–8) due to inter-particle voids. The thermal stability improvement of the material in the amorphous status caused by addition of the transition metal Nb to the Mo oxide should not have been sufficient to elevate the crystallization temperature beyond that required to completely remove the mesoporous template for these samples with x = 1–8, forming inter-particle voids in spite of mesopores. And the decrease on Nb concentration should have decreased the crystallization temperature, forming $Mo_3Nb_2O_{14}$ and MoO_3 for Mo enriched samples with x = 0–3. The pore volume obtained by BJH decreased up to x = 0 due to formation of crystallized $Mo_3Nb_2O_{14}$ and MoO_3, as can be observed in the XRD patterns (Fig. 2) and SEM image of non-porous Mo oxide (Fig. 3). The BJH pore size distributions and BET surface area of samples with different concentrations obtained from N_2 sorption isotherms are summarized in Table 1. The BJH pore size distributions indicate increase on pores sizes for Mo-enriched samples.

3.2. Characterization of acid sites

The acid properties of porous $Nb_xMo_{(10-x)}$ oxides (x = 3, 5, 7, and 10) were evaluated by NH_3 temperature-programmed desorption (NH_3-TPD) and Fourier transform infrared (FT-IR) spectroscopic measurements of adsorbed pyridine. The NH_3-TPD profiles for porous $Nb_xMo_{(10-x)}$ (x = 3, 5, 7) exhibited a broad main peak at 435–445 K (Fig. 5). The order of acid strength of the porous $Nb_xMo_{(10-x)}$ oxides (x = 3, 5, 7) increased with increasing Mo oxide concentration. The main peak was observed at 435 K for porous Nb_7Mo_3 oxide (0.29 mmol g^{-1}), at 440 K for porous Nb_5Mo_5 oxide (0.27 mmol g^{-1}), and at 445 K for porous Nb_3Mo_7 oxide (0.24 mmol g^{-1}).

Table 1
Structural properties of mesoporous $Nb_xMo_{(10-x)}$ oxides.

Mesoporous $Nb_xMo_{(10-x)}$ oxides	S_{BET} (m^2 g^{-1})	Pore size (nm)	Pore volume (mL g^{-1})
Nb_0Mo_{10}	21	–	–
Nb_1Mo_9	43	18.6	0.15
Nb_2Mo_8	52	13.9	0.16
Nb_3Mo_7	57	13.3	0.20
Nb_4Mo_6	68	13.9	0.20
Nb_5Mo_5	70	10.6	0.19
Nb_6Mo_4	77	12.1	0.20
Nb_7Mo_3	81	13.9	0.22
Nb_8Mo_2	99	10.6	0.24
Nb_9Mo_1	166	8.0	0.29
$Nb_{10}Mo_0$	200	7.0	0.35

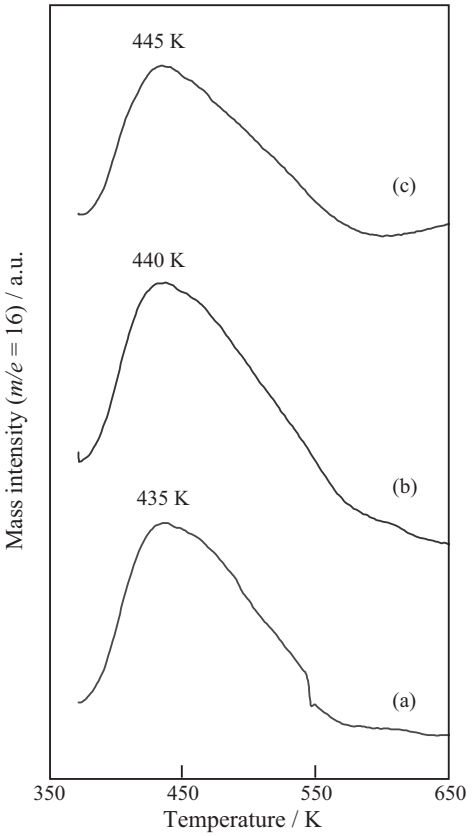

Fig. 5. NH_3-TPD (m/e = 16, 10 K min^{-1}) curves for porous (a) Nb_7Mo_3, (b) Nb_5Mo_5, and (c) Nb_3Mo_7.

The acid properties of $Nb_xMo_{(10-x)}$ oxides (x = 3, 5, 7, and 10) were also evaluated by probing the vibrational spectra of adsorbed pyridine using IR spectroscopic measurements, as shown in Fig. 6. $Nb_xMo_{(10-x)}$ oxides (x = 3, 5, 7, and 10) samples were confirmed to posses Lewis acid site 1440 cm^{-1} and Brønsted acid site 1532 cm^{-1}. The IR spectroscopic measurements indicated that the peak intensity of the bond at 1532 cm^{-1}, attributed to pyridinium ions formed on Brønsted acid sites [12,13,25–27], was enhanced by increasing the Mo content. The increase in Brønsted acid sites

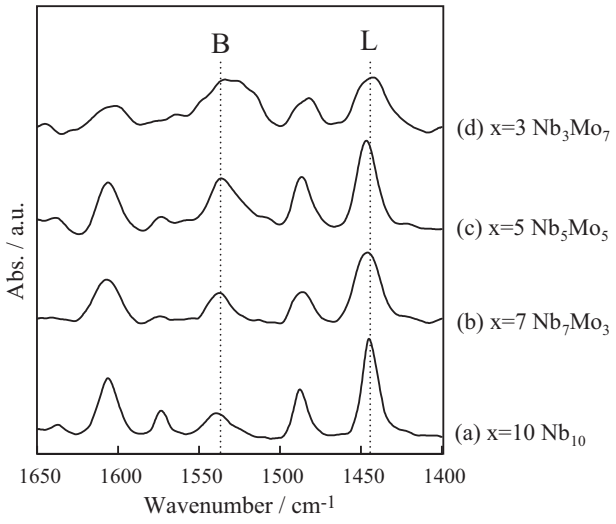

Fig. 6. FT-IR spectra for pyridine adsorbed porous (a) Nb, (b) Nb_7Mo_3, (c) Nb_5Mo_5, and (d) Nb_3Mo_7 oxides (B, Brønsted acid site; L, Lewis acid site). Assignments: 1532 cm^{-1} (Brønsted acid site), 1435 cm^{-1} (Lewis acid site).

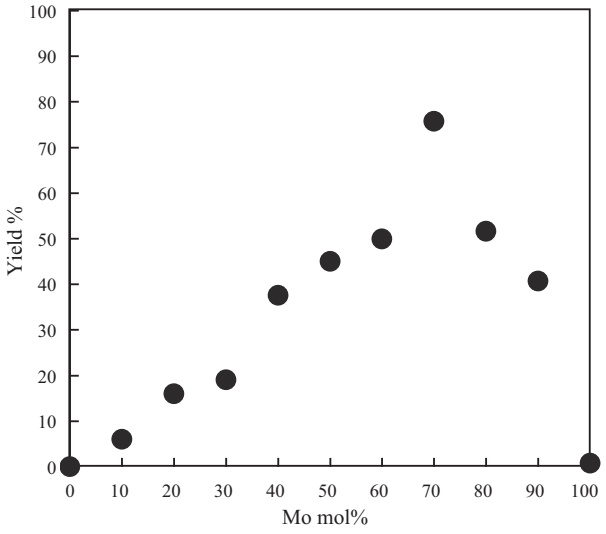

Fig. 7. (a) Friedel–Crafts alkylation of anisole over porous $Nb_xMo_{(10-x)}$ oxides (reaction conditions: anisole (100 mmol), benzyl alcohol (10 mmol), catalyst (0.2 g), 373 K, 1 h).

corresponded with the model structure of a binary oxide for chemically mixed oxides. The excess of a negative charge caused by increase of Mo concentration should have generated the Brønsted acid sites.

3.3. Acid-catalyzed reactions

The acid catalyzed reactions were tested on porous $Nb_xMo_{(10-x)}$ oxides using liquid-phase Friedel–Crafts alkylation of anisole with benzyl alcohol. A plot of the product yield for different Nb and Mo contents in the Friedel–Crafts alkylation of anisole, reacted for 1 h at 373 K is shown in Fig. 7. Variation of the Nb and Mo content resulted in remarkably different reaction rates of benzylanisole formation in alkylation. The reaction rates increased gradually with increasing Mo content, starting from 0% yield for porous Nb oxide and reaching the highest alkylation yield (75.7% of benzylanisole) for porous Nb_3Mo_7 oxide. The yield decreased drastically for non-porous oxide samples with x from 2 to 0, reaching 0% for Mo oxide. The Mo enriched samples show formation of $Mo_3Nb_2O_{14}$ and MoO_3 with no acidity and low surface areas, resulting in the decrease of catalytic activities. The TOF (h^{-1}) values (Table 2) obtained from the rate of produced benzylanisole (1 h) and acid amount of porous $Nb_xMo_{(10-x)}$ oxides also increase gradually for Mo enriched samples: Nb_7Mo_3 (33 h^{-1}) < Nb_5Mo_5 (83 h^{-1}) < Nb_3Mo_7 (158 h^{-1}). This increase in the TOF indicates that the acid sites on porous Nb_3Mo_7 have higher activity than that of porous Nb_7Mo_3 and Nb_5Mo_5 oxides. Both the reaction yield and TOF (h^{-1}) increased for Mo-enriched porous $Nb_xMo_{(10-x)}$ oxide samples, consistent with the acid strength determined by NH_3-TPD and with the increase in Brønsted acid sites, which promotes the Friedel–Crafts alkylation reaction [28], observed by IR spectroscopic measurements.

The acid catalytic activities of porous Nb–Mo oxides for Friedel–Crafts alkylation were also compared to those of conventional solid acids. The acid concentration and surface area of the tested solid acids and the results of the Friedel–Crafts alkylation of anisole are summarized in Table 2. Bulk (Non-porous) Nb_2O_5–MoO_3 oxides prepared from $Nb_2O_5{\bullet}nH_2O$ and $(NH_4)_6Mo_7O_{24}{\bullet}4H_2O$ with different Nb–Mo concentrations exhibited lower reaction yield compared with porous $Nb_xMo_{(10-x)}$ oxides, especially much different between bulk Nb_3Mo_7 oxide and porous Nb_3Mo_7 oxide.

After the reaction, ortho-benzylanisole, para-benzylanisole, and dibenzylether were formed. The selectivity of ortho-benzylanisole via para-benzylanisole observed for porous $Nb_xMo_{(10-x)}$ oxides for Friedel–Crafts alkylation gradually increased with increasing Mo content (38.9, 42.3, and 44.6% for porous Nb_7Mo_3, Nb_5Mo_5, and Nb_3Mo_7 oxides, respectively). The same selectivity of *o*-benzylanisole was observed for bulk Nb_2O_5–MoO_3 (Nb_7Mo_3, Nb_5Mo_5, Nb_3Mo_7) oxide (39.0, 40.1 and 43.8%). The variation of selectivity was probably not caused by the porous structure, but by variations of the acid properties (Brønsted acid and Lewis acid sites) due to changing Nb and Mo concentrations [23,24]. The selectivity for dibenzylether, a by-product of benzyl alcohol, was 13%, 10%, and 7% for porous Nb_7Mo_3, Nb_5Mo_5, and Nb_3Mo_7 oxides respectively. These results are consistent with the IR spectroscopic measurements results, which increase on Brønsted acid sites 1532 cm^{-1} promotes decrease on selectivity of dibenzyl ether, a by-product formed by the Lewis acids. However, dibenzyl ether is also a good alkylating agent, and its concentration decreased as it was consumed, along with the benzyl alcohol, at the end of the alkylation reaction.

Considering the similarity between the acid properties of bulk Nb_2O_5–MoO_3 and porous $Nb_xMo_{(10-x)}$ oxides, the decrease on reaction yield of Mo-enriched bulk Nb_2O_5–MoO_3 oxides should have been caused by the surface area reduction. The surface areas of bulk oxides decrease about 20 times from bulk Nb_7Mo_3 (60 $m^2\,g^{-1}$) to bulk Nb_3Mo_7 (3 $m^2\,g^{-1}$). Therefore the formation of porous structure for Mo-enriched samples (Nb_3Mo_7 and Nb_5Mo_5) should have

Table 2
Friedel–Crafts alkylation of anisole over several solid acid catalysts.

Catalyst	S_{BET} ($m^2\,g^{-1}$)	Acid Amount (mmol g^{-1})	Alkylation of anisole[a]		
			Yield (%)	Selectivity of *o*-benzylanisole (%)[b]	TOF (h^{-1})[c]
Mesoporous Nb_3Mo_7	57	0.24	75.7	44.6	158
Mesoporous Nb_5Mo_5	70	0.27	45.0	42.3	83
Mesoporous Nb_7Mo_3	81	0.29	19.1	38.9	33
Mesoporous Nb	200	0.54	N.D.	N.D.	N.D.
Bulk Nb_3Mo_7	3	0.04	6.9	43.8	86
Bulk Nb_5Mo_5	16	0.10	8.9	40.1	45
Bulk Nb_7Mo_3	60	0.16	17.0	39.0	53
$Nb_2O_5{\bullet}nH_2O$	128	0.40	N.D.	N.D.	N.D.
H-beta[d]	420	1.0	30.6	42.1	15
Amberlyst-15	50	4.8	42.1	45.0	4
Nafion NR50	0.02	0.9	42.3	49.2	24

[a] Reaction conditions: anisole (100 mmol), benzyl alcohol (10 mmol), catalyst (0.2 g), 373 K, 1 h.
[b] Selectivity (%) = (*o*-benzylanisole)/(*o*-benzylanisole + *p*-benzylanisole) × 100.
[c] Calculated from the rate of produced benzylanisole (1 h) and acid amount.
[d] SiO_2/Al_2O_3 = 25, JRC-Z-HB25; N.D., not detected.

helped to maintain the high porous surface area, resulting in high activity for porous oxides.

The high catalytic performance of porous Nb_3Mo_7 oxide was due to the high surface area and formation of strong Brønsted acid sites by the isomorphous replacement of Nb^{5+} by higher-valence Mo^{6+} cations in these Mo-enriched samples like that observed at MoO_3/ZrO_2 [29]. It is reported that replacement of ZrO_2 by MoO_3 forms acids sites similar to that of SO_4/ZrO_2 [29] with strong acid sites. The highest activity of MoO_3/ZrO_2 has been obtained at the range of surface molybdenum densities, which maximizes the quantity of amorphous surface molybdenum species [30]. Similar to MoO_3/ZrO_2 and Nb_2O_5–MoO_3, formation of strong Brønsted acid sites could be observed at IR spectroscopic measurements results of porous $Nb_xMo_{(10-x)}$ oxides. The Brønsted acid sites could have formed led to the high surface molybdenum densities in niobium matrix. Higher concentrations of Mo oxide formed the crystallized MoO_3 and $Mo_3Nb_2O_{14}$ decreasing the reaction rate for Mo rich samples (x = 0–2).

4. Conclusion

Porous $Nb_xMo_{(10-x)}$ oxides were found to function as highly active mixed metal oxide solid acid catalysts for Friedel–Crafts alkylation, exceeding the reaction rate of non-porous Nb_2O_5–MoO_3 oxide. Different from mesoporous $Nb_xW_{(10-x)}$ and $Ta_xW_{(10-x)}$ oxides, $Nb_xMo_{(10-x)}$ oxide formed mesopores only for Nb rich samples (x = 9–10), forming a large pores formed by inter-particle voids for samples with x from 3 to 8. The formation of crystallized MoO_3 and $Mo_3Nb_2O_{14}$ were observed in Mo-rich samples (x = 0–4). The Nb–Mo interaction seems to be responsible for the formation of inter-particle voids and crystallized structures. The reaction rate and acid strength increased gradually with the addition of Mo, reaching the highest reaction rate with porous Nb_3Mo_7 oxide, which exceeded the reaction rate of ion-exchange resins, zeolites, and non-porous metal oxide. The high catalytic performance of porous Nb_3Mo_7 oxide was due to the formation of strong Brønsted acid sites and high surface area.

Acknowledgments

This work was supported by the Development in a New Interdisciplinary Field Based on Nanotechnology and Materials Science program of the Ministry of Education, Culture, Sports, Science and Technology (MEXT) of Japan and the Global Center of Excellence Program for Chemistry.

References

[1] I. Nowak, M. Ziolek, Chem. Rev. 99 (1999) 3603.
[2] K. Tanabe, S. Okazaki, Appl. Catal. 133 (1995) 191.
[3] K. Hanaoka, T. Takeuchi, T. Matsuzaki, Y. Sugi, Catal. Today 8 (1990) 123.
[4] K. Hanaoka, T. Takeuchi, T. Matsuzaki, Y. Sugi, Catal. Lett. 5 (1990) 13.
[5] K. Ogasawara, T. Iizuka, K. Tanabe, Chem. Lett. (1984) 645.
[6] O. Okazaki, H. Harada, Chem. Lett. (1988) 1313.
[7] J.J. Spivey, M.R. Gogate, J.R. Zoeller, R.D. Colberg, Ind. Eng. Chem. Res. 36 (1997) 4600.
[8] T. Ushikubo, K. Wada, Appl. Catal. 67 (1990) 25.
[9] L. Li, Y. Yoshinaga, T. Okuhara, Phys. Chem. Chem. Phys. 1 (1999) 4913.
[10] K. Shibata, T. Kiyoura, J. Kitagawa, T. Sumiyoshi, K. Tanabe, Bull. Chem. Soc. Jpn. 46 (1973) 2985.
[11] K. Tanabe, T. Sumiyoshi, K. Shibata, T. Kiyoura, J. Kitagawa, Bull. Chem. Soc. Jpn. 47 (1974) 1064.
[12] K. Yamashita, M. Hirano, K. Okumura, M. Niwa, Catal. Today 118 (2006) 385.
[13] M. Hino, M. Kurashige, K. Arata, Catal. Commun. 5 (2004) 107.
[14] K. Okumura, K. Yamashita, M. Hirano, M. Niwa, Chem. Lett. 34 (2005) 716.
[15] K. Okumura, K. Yamashita, M. Hirano, M. Niwa, J. Catal. 234 (2005) 300.
[16] Y.-Y. Huang, T.J. McCarthy, W.M.H. Sachtler, Appl. Catal. A 148 (1996) 135.
[17] M. Chidambaram, D. Curulla-Ferre, A.P. Singh, B.G. Anderson, J. Catal. 220 (2003) 442.
[18] S.M. Landge, M. Chidambaram, A.P. Singh, J. Mol. Catal. A: Chem. 213 (2004) 257.
[19] C.-C. Hwang, C.-Y. Mou, J. Phys. Chem. C 113 (2009) 5212.
[20] Y. Rao, M. Trudeau, D. Antonelli, J. Am. Chem. Soc. 128 (2006) 13996.
[21] Y. Rao, J. Kang, D. Antonelli, J. Am. Chem. Soc. 130 (2008) 394.
[22] J. Kang, Y. Rao, M. Trudeau, D. Antonelli, Angew. Chem. Int. Ed. 47 (2008) 4896.
[23] C. Tagusagawa, A. Takagaki, A. Iguchi, K. Takanabe, J.N. Kondo, K. Ebitani, S. Hayashi, T. Tatsumi, K. Domen, Angew. Chem. Int. Ed. 49 (2010) 1128.
[24] C. Tagusagawa, A. Takagaki, A. Iguchi, K. Takanabe, J.N. Kondo, K. Ebitani, T. Tatsumi, K. Domen, Chem. Mater. 22 (2010) 3072.
[25] E.P. Parry, J. Catal. 2 (1963) 371.
[26] T.R. Hughes, H.M. White, J. Phys. Chem. 71 (1967) 2192.
[27] M. Hino, M. Kurashige, H. Matsuhashi, K. Arata, Appl. Catal. A 310 (2009) 190.
[28] T. Shishido, T. Kitano, K. Teramura, T. Tanaka, Catal. Lett. 129 (2009) 383.
[29] K. Arata, H. Matsuhashi, M. Hino, H. Nakamura, Catal. Today 81 (2003) 17.
[30] S.K. Maity, M.S. Rana, B.N. Srinivas, S.K. Bej, G. Murali Dhar, T.S.R. Prasada Rao, J. Mol. Catal. Chem. 153 (2000) 121.